Clays and Clay Minerals, Vol. 48, No. 2, 151–158, 2000.

Ti-BEARING PHASES IN THE HUBER FORMATION, AN EAST GEORGIA KAOLIN DEPOSIT

PAUL A. SCHROEDER AND JASON SHIFLET†

University of Georgia, Department of Geology, 210 Field Street, Athens, Georgia 30602-2501, USA

Abstract—Six kaolin samples from the Lower Tertiary Huber Formation near Wrens, Georgia were analyzed using transmission electron microscopy (TEM), electron diffraction (ED), powder X-ray diffraction (XRD), chemical analysis, and magnetic susceptibility to characterize the Ti-bearing phases. Selected samples were treated with 5 M NaOH to remove kaolinite and concentrate the Ti-bearing phases for additional analysis. TiO_2 content in the bulk fraction ranges from 1.2 to 5.4 wt. %. There are at least three Ti-bearing phases, including anatase, rutile, and a poorly defined nanocrystalline form. Anatase is most abundant and is commonly found with {010} faces in association with kaolinite edge and basal faces. The nanocrystalline form occurs at 0–1 wt. %, and rutile occurs in trace amounts. Bulk XRD analysis correlates well with the bulk TiO_2 chemical measurements. Average anatase unit-cell parameters are $a = 0.37908 \pm 0.0002$ nm and $c = 0.951 \pm 0.001$ nm. These parameters indicate an approximate chemical formula of $Fe^{3+}_{0.05}Ti^{4+}_{0.95}O_{1.95}(OH)_{0.05}$.

The distribution of TiO_2 content as a function of depth may be useful to obtain original grain-size variations associated with relative sea-level changes responsible for the deposition of the Huber Formation. Evidence for original depositional sediment properties can be seen in the occurrence of pseudomorphic replacement of micas and fecal pellets by kaolinite. Additional evidence for post-depositional changes includes the sub-micrometer euhedral character and low Fe content of the anatase (relative to soil-derived anatase). These observations for the Huber Formation are consistent with a previously published theory for kaolin genesis that includes biomineralization of originally coarser-grained aluminosilicates into a kaolinite-rich ore body.

Key Words—Anatase, Georgia, Huber Formation, Kaolinite, Rutile, TiO_2, Titanium, X-ray Diffraction.

INTRODUCTION

Ti-bearing phases are ubiquitous in Georgia kaolin deposits (Weaver, 1976; Hurst, 1997). Interest in these Ti-bearing phases is related to the potentially deleterious effect that Ti phases have on the color of processed clay products. The efficiency of removal of these impurities is an integral factor in the economics of clay processing. Also, it is desirable to examine the distribution and occurrences of Ti phases relative to current theories on the origin of kaolin deposits found in the Coastal Plain of the southeastern United States (*e.g.,* see Dombrowski, 1993 and Hurst and Pickering, 1997) and the classification of these deposits. The purpose of this paper is to document the crystal-chemical properties of Ti-bearing phases in an east Georgia kaolin deposit, to examine the spatial variation of Ti content, and to compare these results to theories on kaolin genesis.

Background relating to the formation of east Georgia deposits

The kaolinite-bearing Huber Formation of east Georgia was formed from metamorphic- and igneous-derived silicate minerals and *in situ* weathering products from the Piedmont. These sediments were probably transported by rivers to Late Cretaceous and Early Tertiary inter-deltaic, estuaries, and back-barrier island localities. At the same time, relative sea-level changes provided sedimentary depositional settings favorable for the accumulation of lithologic units, such as the lens-shaped geometry of the present-day deposits. The settling of suspended river sediments as they encountered estuarine waters occurred by flocculation and by suspension-feeding organisms (*i.e.,* formation of fecal pellets). The latter is inferred by framboidal pyrite and kaolinite pseudomorphs of fecal pellets. Pyrite occurs in association with marine waters (Berner, 1970) and suspension-feeders are known to proliferate in estuarine and coastal waters. After the deposition of the Huber Formation, the shoreline repeatedly transgressed and regressed, thereby leaving a sequence boundary overlain by smectitic marine clay and quartz-rich sandstone deposits. These younger formations (Twiggs Clay and Clinchfield Sand, respectively) are collectively part of the Miocene Barnwell Group. At some localities, multiple kaolin deposits of the Paleocene to Eocene Huber Formation occur and are separated by deposits similar to those of the Barnwell Group. Stratigraphic details and previous research have been summarized by Hurst and Pickering (1997).

Variables influencing the Ti content of the sediment supplied to the sites of deposition include: (1) the composition of the parent rock, which contains Ti-bearing phases such as biotite, amphibole, magnetite, ilmenite, rutile, anatase, and titanite (Deer *et al.,* 1992), (2)

† Present address: Zapata Engineering, P.A., 1100 Kenilworth Ave., Suite 104, Charlotte, North Carolina 28204, USA.

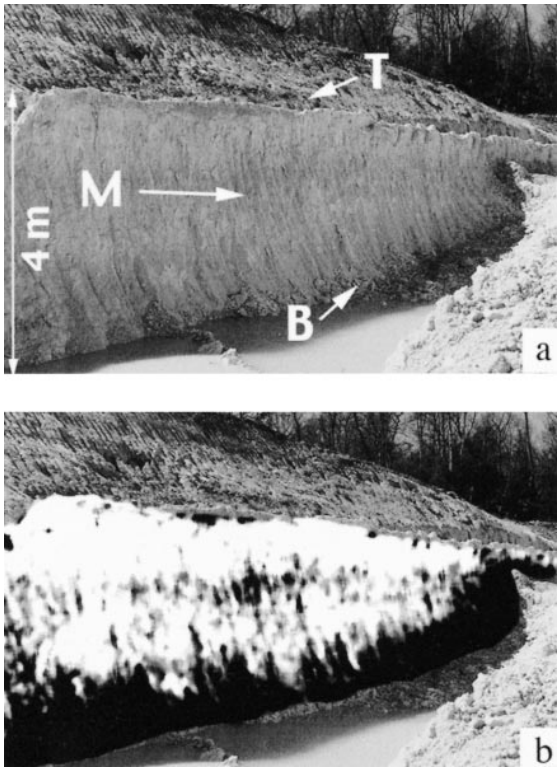

Figure 1. (a) Outcrop view of the Jeffersonville Member of the Huber Formation. T, M, and B mark collection sites for the top, middle, and bottom samples, respectively. (b) This image was created by selecting pale yellow pixels in a digitized color version of the above photograph. Selected color pixels were replaced by white pixels, then the image was converted to a gray-scale and contrast enhanced. The central dark band highlights Ti-enriched zones.

changes in climatic regime (temperature and water infiltration) as it affects vegetation and rates of chemical alteration of crystalline rock by selective dissolution, (3) long-term effects of river and littoral currents by hydraulic sorting of sediments (Doyle *et al.*, 1983), and (4) tectonic changes, including uplift and subsidence rates and how such changes affect colluvial transport of source material (Pavich, 1989).

Variables influencing post-depositional Ti content of the sedimentary deposits include: (1) early diagenetic changes to the sediments including the oxidation of Fe^{2+}- and Ti-bearing minerals and subsequent Fe sequestration into pyrite during bacterial sulfate reduction (Raiswell and Canfield, 1996), (2) oxidation and dissolution of Fe^{2+}- and Ti-bearing minerals in association with exposure to meteoric waters during times of subaerial exposure, (3) changes in climatic regime as temperature and water infiltration affect vegetation and rates of biogeochemical reactions, and (4) tectonic changes, including uplift and subsidence rates and how these changes affect the regional groundwater pathways (Hurst and Pickering, 1997). Local and regional variations in kaolin lithologies are attributed to the intensity and duration of any of the above factors.

MATERIALS AND METHODS

Samples were collected from two sites near Wrens, Georgia. The first suite was collected by the J.M. Huber Corporation from subsurface core material sampled at 2-foot (61 cm) intervals. Six samples from the first suite were selected for detailed crystal-chemical analysis. A second suite of three samples was also collected at a strip mine (see Figure 1) operated by the J.M. Huber Corporation. Samples were disaggregated and passed through a 45-μm sieve. Bulk-sample K, Fe, and Ti analyses were made by preparing pressed pellets and using X-ray fluorescence spectroscopy (XRF).

Magnetic-susceptibility measurements were made using a Johnson-Matthey magnetic-susceptibility balance. The balance makes a direct mass-susceptibility measurement after calibration with a known reference material [$HgCO(SCN)_4$]. The mass susceptibility (χ_g) is defined as the ratio of intensity of the magnetism induced in a substance to the intensity of the applied field divided by the material density. Units are cm^3/g.

Samples were prepared for transmission electron microscopy (TEM) by dispersal of dilute suspension onto a Formvar-coated TEM sample holder (200 mesh copper grid). Dispersion techniques are used to separate mineral grains and to examine isolated particles by TEM. Within these particles, we are interested in examining grain-contact relationships that may have not been affected by the dispersion technique. Thus, these relationships may be representative of those in the clay deposit. Dispersion techniques are complicated by artifacts, such as clumping during drying of the dilute suspensions. Consequently, we tested three different dispersion procedures. The first involved a mild ultrasonic dispersion of sample material in distilled water. The second involved the addition of a dispersent, sodium meta-phosphate, and the third used a novel electrodispersion technique of Hurst (Shiflet, 1999).

The latter procedure allowed the examination of artifacts possibly induced by the dispersent. The electrodispersion method employs an electric potential across a set of closely spaced Cu TEM sample holders. Immediately before application of the potential, a sample dispersed in distilled water is pipetted between the positive and negative nodes. With application of the potential, the naturally charged surfaces of the particles align for a short period, such that the external electrical forces counter the gravitational and van der Waals forces that cause flocculation. As the particles remain dispersed, the water is slowly removed by the wick action of a narrow piece of filter paper. The comparative TEM results indicate that without dispersion (chemical or electrical) the distilled-water, ultrasonic treatment resulted in significant flocculation and particle aggregation that made TEM viewing difficult.

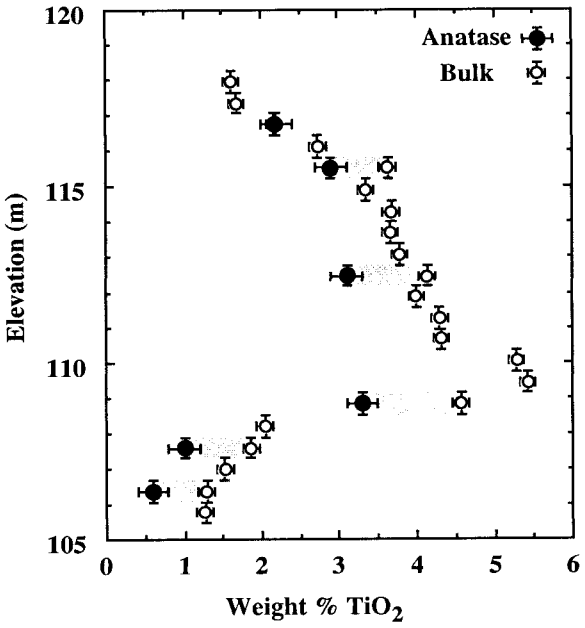

Figure 2. Titanium content (oxide wt. %) *vs.* elevation (m) of sampling. Bulk TiO_2 values (open circles) were determined by XRF and the anatase values (closed circles) were determined by XRD. The shaded areas represent the difference between the bulk TiO_2 and anatase content or ''non-anatase TiO_2''.

There were no observable differences in dispersion efficiency between samples prepared from sodium metaphosphate and samples from the electrodispersion. Both methods yielded good and similar dispersion onto the TEM girds. For ease of sample preparation, subsequent TEM samples were made using the chemical dispersent.

TEM and electron diffraction (ED) analyses were conducted using a Philips model-400 TEM operated at 100 kV. Grids were vacuum-plated with a thin coat of carbon both before and after sample mounting. A separate sample of magnetically susceptible material concentrated from the east Georgia processing operations of Huber was also examined by high-resolution TEM and energy dispersive analysis (EDS).

Samples of the core material were size separated via centrifugation into four ranges, based on an equivalent spherical-diameter particle with a density of 2.65 g/cm^3 (Hathaway, 1956). Size ranges included <0.05, 0.05–2.0, 2.0–10, and 10–45 μm.

Powder X-ray diffraction (XRD) analyses were conducted using a Scintag XDS-2000 diffractometer, solid-state detector, and Cu radiation source. Sample mounts were prepared using the back-fill technique. These mounts minimize transparency and sample displacement effects, as discussed by Hurst *et al.* (1997). Quantitative analyses for anatase content of the bulk samples and their respective size fractions were performed using the internal standard method of Chung (1974). Experimental parameters included a scan step of 0.01° and preset time of 10 s per step (0.06° per min). Reference intensity ratios were determine for the anatase (101) and the (100) reflection of the ZnO internal standard by using synthetic anatase (whose peak shapes showed that the coherent scattering domain sizes were comparable to those in the natural samples). Measurements for quantitative analysis were made using intensities of reflections from samples mixed with 20 wt. % ZnO.

XRD data were background corrected using a linear function and the *least-squares* fit using a Voight function for peak shapes (Krumm, 1998). The anatase (101) peak maximum was measured relative to the position of the ZnO (100) in the sample with highest abundance of anatase. Overlap of the kaolinite (002) and anatase (101) required fixing the position of the anatase peak maximum during optimization, particularly when anatase abundance diminished. The ZnO reflections were previously calibrated via a 50/50 mixture with NIST SRM640b (silicon powder XRD line reference).

To evaluate differences in Fe substitution in the natural anatase structure by XRD, calculated diffraction patterns were generated with and without Fe occupying the Ti site (Downs *et al.,* 1993). Calculated patterns for anatase using 0 and 5% Fe-occupancy factors revealed relative differences of 0.01% between the integrated (101) peak intensities. Because this is an order of magnitude less than observed variations in the analytical precision for a single sample, this effect was negligible.

Indexing and unit-cell refinements for anatase in the six samples were obtained by concentrating the oxides using the selective NaOH kaolinite-dissolution method (Kampf and Schwertmann, 1982, as modified by Singh and Gilkes, 1991). Peak positions were determined from $K\alpha_2$ stripped data and then corrected using the ZnO internal standard. Anatase (101), (103), (004), (112), (200), (105), and (211) reflections were used as input to the Appleman-Evans program adapted for microcomputers by Benoit (1987) for indexing of powder-diffraction data and *least-squares* refinement of unit-cell dimensions. Triplicate analysis of the same sample resulted in a precision of ±0.00005 nm for the *a* and *c* cell dimensions. The Appleman-Evans program and the analytical method described in Cullity (1978, p. 337) produced similar results, and the latter was used as a check for the computer program.

RESULTS

Chemical and XRD analyses

Chemical analysis of the bulk-core material show depth-related Ti and K trends that are antithetic with Fe content (Figures 2 and 3). TiO_2 content near the base of the deposit is relatively low (~1%). The TiO_2

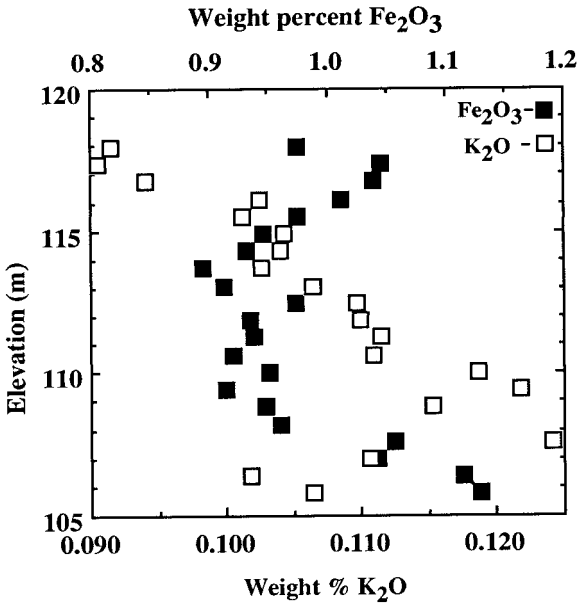

Figure 3. Bulk Fe_2O_3 (closed squares) and K_2O content (open squares) *vs.* elevation (m) of sampling.

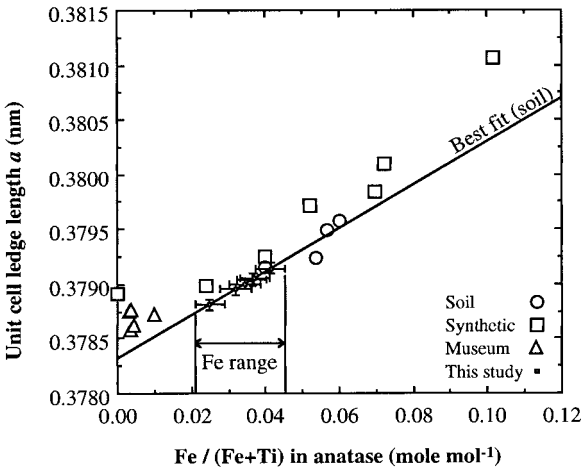

Figure 4. Anatase *a* unit-cell edge length for samples in this study. Also plotted are *a* values and independently measured mole fraction Fe substitution for anatase samples studied by Schwertmann *et al.* (1995). The line represents a linear best-fit solution to soil derived data only. Placement of the observed *a* values for each sample from this study suggests that the mole fraction Fe content of anatase ranges from 0.020 to 0.045.

content then increases towards the middle of the deposit (~7%) and finally, decreases near the top (~2%). Fe concentrations trend in a quasi-antithetic fashion with Ti, with Fe content being the lowest in the middle part of the depositional unit. Magnetic mass-susceptibility (χ_g) measurements range from 1.28 to 0.92 $\times$ 10^{-6} cm^3 g^{-1} and correlate positively with Fe content ($\chi_g = -0.86 \times 10^{-6} + 1.92 \times 10^{-6}$ wt. % Fe, $r^2 = 0.79$).

Quantitative XRD analysis of the bulk material shows that anatase constitutes 80–100 wt. % of the total TiO_2 content. The difference between the anatase and total TiO_2 is hereafter referred to as ''non-anatase TiO_2'' and is illustrated by the shaded regions in Figure 2. The TiO_2 and Fe_2O_3 trend observed in the top, middle, and bottom samples of the outcrop are similar to the core samples. The significance of the coincidence between these two trends requires more comprehensive study of the Ti content *versus* depth relations throughout the east Georgia kaolin district.

The high reflectivity of the outcrops makes it difficult to see subtle coloration changes (Figure 1a). A color-based, contrast-enhanced photograph (Figure 1b) reveals layers enriched in Ti content. The light areas in the enhanced portion of Figure 1b are pale yellow (2.5Y 8/2) in color and the central dark area is yellow (7/6 10YR). The bottom portion of the enhanced area is a shadowing effect. The top most portion (~1 m) of the outcrop in Figure 1a and 1b is unobserved because it was removed by the mining operation.

Qualitative XRD analysis of the kaolinite-extracted samples revealed that anatase, quartz, mica, and rutile comprise the bulk of the residue. Seven anatase reflections are distinguishable in the XRD patterns. Results for the six intensively studied samples are plotted in Figure 4 and show that the value of *a* ranges from 0.37881 to 0.37914 nm. Using the method described in Cullity (1978, p. 337) the average unit-cell parameters for the six samples are $a = 0.37908(5)$ nm and $c = 0.95086(5)$ nm. These anatase lattice parameters approximate a chemical formula of $Fe^{3+}_{0.05}Ti^{4+}_{0.95}O_{1.95}(OH)_{0.05}$.

TEM analyses

Anatase was the most abundant Ti-bearing phase observed by TEM. Figure 5a shows the typical pseudocubic habit. Based on 100 observations per sample, anatase crystals ranged between 0.10–0.05 μm and all appeared pseudocubic to tabular. Electron-diffraction patterns (Figure 5) show anatase crystals most often occurred with *c** or *a** perpendicular to the electron beam. The extent to which anatase {100} and {001} faces associate with the kaolinite (001) surfaces or the kaolinite edge (010) and (130) surfaces was about equal. The tedious task of verifying each anatase crystal orientation with electron diffraction precluded a rigorous study of crystallographic orientations, therefore morphologic criteria were employed. Two general grain-contact relationships observed included the anatase {010} in contact with the kaolinite non-basal edges and the anatase {010} in contact with the kaolinite basal surfaces. Associations between the anatase (001) and kaolinite surfaces are less common. EDS analysis of anatase revealed Fe as a minor constituent (Shiflet, 1999), but the lack of calibration data and

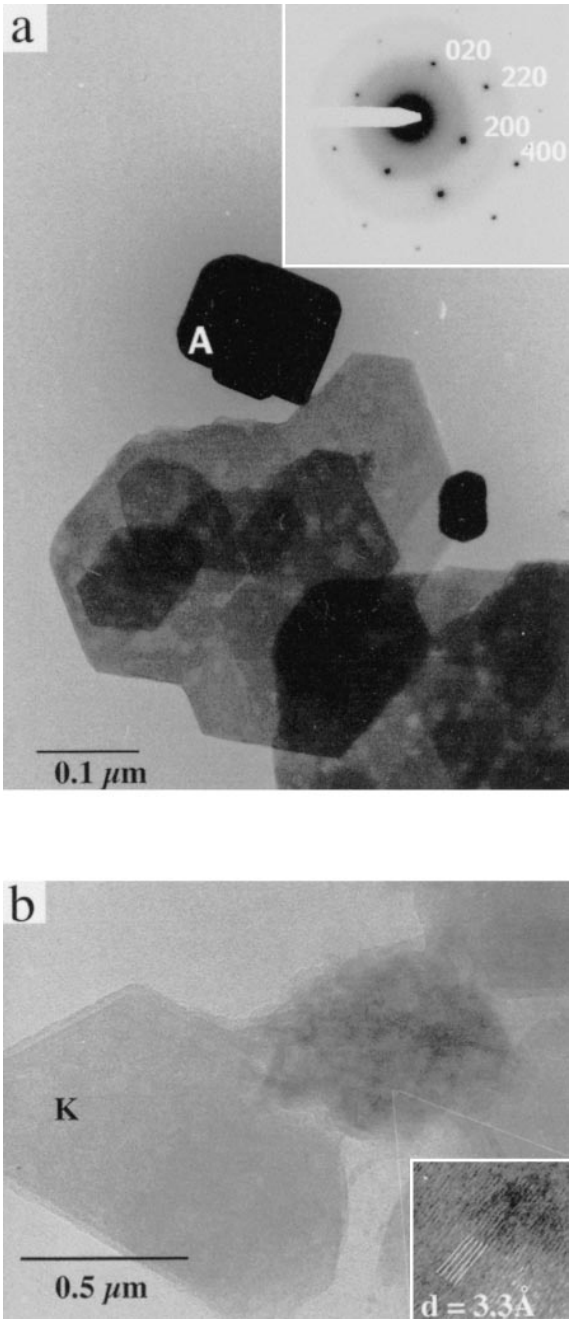

Figure 5. (a) TEM photograph of anatase (**A**) oriented with (010) face adjacent to kaolinite (**K**) edge. Inset shows electron-diffraction pattern with the a^* and b^* axes in the plane of the page. (b) TEM photograph of heterogeneous Ti-bearing particle. Inset shows high-resolution lattice-fringe images with parallel lines overlain to show the regular spacings (0.33 nm).

geometric constraints prevented EDS-based quantification of the Fe content.

The second most abundant Ti-bearing phase appears as highly mottled heterogeneous particles typically 0.1 μm in diameter (Figure 5b). Electron diffraction does not reveal a strong coherent spot pattern. EDS analysis shows the coexistence of Ti, Fe, Al, and Si, along with minor amounts of S and K (Shiflet, 1999). Nanocrystalline regions within the heterogeneous particles produced lattice-fringe images (Figure 5b). The fringes repeat at a distance of ~0.33 nm. These observations are consistent with several possible interpretations. The mottled appearance suggests that either the particles represent single grains with dissolution pitting or the particles represent nanocrystalline aggregates (Banfield *et al.*, 1998). The chemical data suggest the coexistence of rutile or anatase or titanite and illitic clay, or the degraded remains of muscovite or biotite. The lattice-fringe spacing of 0.33 nm approximates the rutile (110), anatase (011), titanite (211), or biotite-$2M_2$ (006) spacings. There exists a positive correlation ($r^2 = 0.5$) between K_2O content values in Figure 3 and corresponding non-anatase TiO_2 values in Figure 2. If the poorly defined Ti phase is a vestige of biotite, then biotite was probably a precursor. The presence of Fe and S also suggests pyrite as a component.

DISCUSSION

Theories relating to the origin of east Georgia kaolin deposits suggest that variations in (1) sediment provenance, (2) erosion rates, (3) sediment transport, and (4) post-depositional diagenetic/weathering alterations are important factors. Variations in the amount and types of Ti-bearing phases in the kaolin deposits are more broadly attributed to pre-depositional factors (herein defined as influenced by factors 1 through 3 above) and post-depositional factors (herein defined as influenced by factors in 4 above).

Evidence from this study and others (*e.g.*, Hurst and Pickering, 1997) strongly suggest that the kaolin deposits experienced significant post-depositional alteration. The occurrence of finely disseminated hematite and goethite throughout the deposits is probably related to the recent oxidation of early diagenetic framboidal pyrite. Framboids are an indicator of a seawater-influenced depositional environment and sulfate-reducing (anoxic) conditions below the sediment-water interface (Berner, 1970). Relict mica and fecal pellet forms (Figure 6) support the study of Hurst and Pickering (1997) that subsurface biogeochemical processes further altered the deposits to their present state. If the kaolin deposits have undergone significant recrystallization, then an important question is to what degree have the Ti-bearing phases been redistributed within the deposit?

The geochemical properties of Ti^{4+} make it highly insoluble, owing in part to an ionic potential of 5.9 (defined as charge/ionic radius). Thus Ti^{4+} is an amphoteric ion with both acid and base properties (Shaw, 1960). Soluble radical complexes involving Ti^{4+} tend to form insoluble oxides. Assuming minimal transmi-

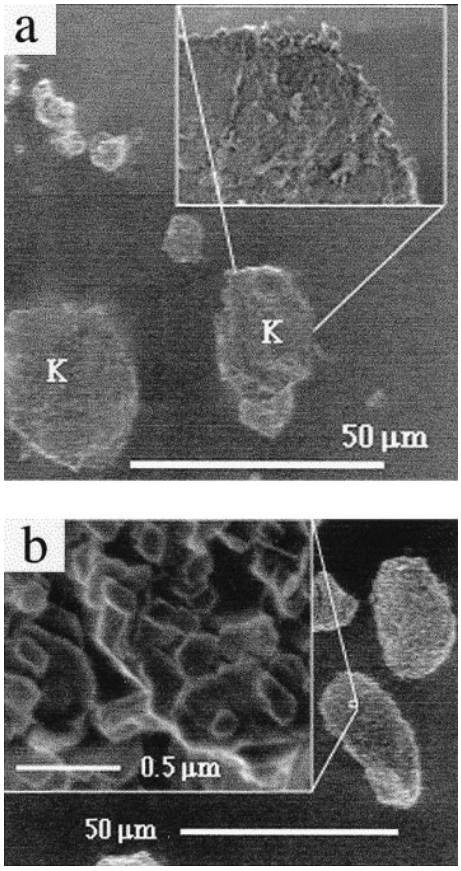

Figure 6. Scanning-electron micrographs of particles fractionated from 10 to 45 μm. These silt-size grains have precursor morphologies of mica flakes (a) and fecal pellets (b). Inset of (a) shows pseudohexagonal faces. A higher magnification image of (a) is similar to the inset of (b), which shows that both particles are composed of kaolinite (K).

gration of Ti, it remains unclear if the Ti-bearing phases observed in this study are authigenic or allogenic constituents.

Figure 4 shows a best-fit line through the observed *a* unit-cell lengths as a function of Fe substitution for four samples of natural anatase from Schwertmann *et al.* (1995) to estimate Fe content for the anatase samples studied here. The resulting values of 0.020–0.045 mol mol^{-1} in the anatase is relatively small and Fe content appears lower than the soil-derived Fe-bearing anatase (Schwertmann *et al.*, 1995). With the small size of the anatase (~0.1 μm), grains may be transported long distances and deposited without evidence of physical abrasion. The transport of fine euhedral ~0.1-μm particles in modern rivers flowing through the kaolin district was documented by Dodge (1991). Anatase however, was not identified by Dodge (1991) in the river sediments of the Piedmont. Furthermore, anatase was not observed in NaOH-treated iron-oxide concentrates from soils developed in felsic parent rocks of the Piedmont (Melear, 1998). These observations support an authigenic origin for the anatase.

To consider allocthonous effects on the Ti content of the deposit, the density of Ti-bearing minerals (*i.e.*, biotite, amphiboles, magnetite, ilmenite, rutile, anatase, and titanite) must be considered. The density of these minerals ranges from 3.0 to 5.0 g/cm^3. Non-Ti-bearing minerals (*i.e.*, muscovite, quartz, feldspar, and kaolinite) have densities ranging from 2.5 to 3.0 g/cm^3. On average, the densities of Ti-bearing phases are 1.5 times greater than non-Ti-bearing phases. Thus, the hydraulic sorting of these minerals by size and density will affect the heavy-mineral concentrations in the initial deposit. Dydak (1991) showed in a study of sediments off the coast of Virginia that these heavy minerals concentrate in fine-silt fractions. This effect is attributed to more intensive chemical weathering of the heavy minerals in the parent rocks and abrasion of the heavy minerals during transport relative to quartz and muscovite.

The hydraulic equivalence of heavy and light minerals can be used to evaluate the likelihood of anatase being transported and deposited along with framework grains. To a first approximation, a comparison can be made by examining settling velocities using Stoke's Law. Under similar settling conditions, the only effects that are independent are the density differences of the heavy and light particles (ρ_h and ρ_l) and the particle diameters (D_h and D_l). For average densities of ρ_h = 4.0, ρ_l = 2.65, and ρ_{water} = 1.0 g/cm^3, the hydraulic relationship of cotransported grains involves a D_h:D_l ratio of 0.74. Thus, if heavy minerals are transported as 0.1-μm diameter grains, then the diameter of contemporaneously transported light minerals is 0.14 μm. The idea that the original deposit was composed of nearly colloidal particles is untenable, because modern depositional analogs are not observed. Thus deposits, as they are found today, were originally deposited as coarser-grain sediments that have experienced significant dissolution and precipitation of new phases.

Variations in parent-rock composition as it affects the source material of a single vertical profile deposited over a short-time period is less likely to be a causative factor for variations in Ti content. The Huber Formation at our study sites is ~15 m thick. Assuming a typical continental sedimentation rate of 1 m/1000 y, this would require the duration of sedimentation at the study site to be ~15,000 y. The period of deposition for the Huber Formation throughout southeastern North America has likely spanned a much greater time interval and the possibility for site to site differences in Ti content owing to changes in parent rock with time is real.

We propose that Ti-bearing minerals (*e.g.*, ilmenite and biotite) were components of the original deposit, and with concentrations in the finer-silt fraction. Postdepositional oxidation of the Fe^{2+}- and Ti-rich min-

erals during early diagenesis and later weathering events recrystallized the Ti primarily into anatase (Anand and Gilkes, 1984). Assuming that the provenance of the sediment has not changed and that the anatase is authigenic, then the Ti content of the east Georgia kaolin deposits can be used to delineate variations in grain size of the initial deposit. The stratigraphic patterns of Ti content seen in our study are similar to vertical trends in grain size expected during a cycle of relative sea-level change (Walker, 1992).

A single cycle of relative change in sea level begins with a sequence boundary formed during a relative fall in sea level (Walker, 1992). During this lowstand, erosional channel surfaces occur and are then overlain by relatively coarse-grain sediments. Such channel complexes occur throughout the base of the Huber Formation. During the subsequent rise in relative sea level, deeper-water marine facies occur. The sediments preserved in this sequence are predicted to fine upwards. Following the highstand, marine facies are expected to shallow upward, leading to an upward coarsening succession of sediment.

If the relatively immobile Ti-bearing phases track depositional features, then a more systematic regional study of Ti-bearing phases throughout east Georgia would be useful. One mitigating factor in using spatial Ti-content patterns is the potential to concentrate these insoluble phases by mass loss of the alkali and alkaline-earth metals during post-depositional recrystallization. This has the effect of increasing the relative concentration of anatase in the deposits. This effect is probably real; however, there is no way to evaluate the degree of mass loss. The study samples were correlated for relative changes in non-anatase TiO_2, quartz, and mica content. However, no systematic depth-related patterns or relationships with anatase content appear. Perhaps evaluating other insoluble ions (*e.g.*, V, Zr, or Hf) would constrain the problem.

CONCLUSIONS

Evidence from this study is consistent with the genesis theory of Hurst and Pickering (1997) for the Georgian kaolin deposits. This theory involves significant post-depositional dissolution and precipitation reactions. These include: (1) the preponderance of submicron authigenic Fe-bearing anatase as the dominant Ti-bearing phase, (2) the absence of primary Ti-bearing phases known to occur in the source area (except rutile) and, (3) the occurrence of mica and fecal-pellet pseudomorphs composed of kaolinite. Vertical patterns of TiO_2 content in the Huber Formation are consistent with expected original grain-size variations associated with relative cycles in sea level. This concept assumes the hydraulic concentration in heavy minerals in finer silt-sized fractions and minimal transmigration of Ti during weathering and diagenesis. Future work should be directed at testing these assumptions and gaining insight to the magnitude of alkali and alkaline-earth mass-loss effects on concentrating Ti content in kaolin deposits.

ACKNOWLEDGMENTS

This work was generously supported by a grant from the J.M. Huber Corporation to the senior author. It is an outgrowth of the M.S. thesis work of the junior author. Our gratitude is extended to M. Duncan, who contributed to the ideas in this paper. Appreciation is extended to V. Hurst, N. Melear, S. Holland (University of Georgia, Geology), W. Barker (University of Wisconsin), M. Farmer (University of Georgia Center for Advanced Ultrastructural Research), S. Guggenheim, and an anonymous reviewer for their insights and technical assistance.

REFERENCES

Anand, R.R. and Gilkes, R.J. (1984) Weathering of ilmenite in a lateritic pallid zone. *Clays and Clay Minerals,* **32,** 363–374.

Banfield, J.F., Penn, R.L., and Zhang, H. (1998) Defect formation and phase transformation in nanocrystalline titania. *Geological Society of America Meeting, Toronto, Canada, Abstracts with Programs,* Abstract 50550.

Benoit, P.H. (1987) Adaptation to microcomputer of the Appleman-Evans program for indexing and least-squares refinement of powder diffraction data for unit-cell dimensions. *American Mineralogist,* **72,** 1018–1019.

Berner, R.A. (1970) Sedimentary pyrite formation. *American Journal of Science,* **268,** 1–23.

Chung, F.H. (1974) Quantitative interpretation of X-ray diffraction patterns of mixtures. II. Adiabatic principle of X-ray diffraction analysis of mixtures. *Journal of Applied Crystallography,* **7,** 526–531.

Cullity, B.D. (1978) *Elements of X-ray Diffraction.* Addison-Wesly Publishing Co., Inc., Reading, Massachusetts, 555 pp.

Deer, W.A., Howie, R.A., and Zussman, J. (1992) *An Introduction to the Rock-Forming Minerals.* Longman Group Limited, Hong Kong, 696 pp.

Dodge, J.J. (1991) Estuarine transformation of fluvial khandite, coastal Georgia. M.S. thesis, Department of Geology, University of Georgia, Athens, Georgia, 91 pp.

Dombrowski, T. (1993) Theories of origin for the Georgia kaolins: A review. In *Kaolin Genesis and Utilization,* H. Murray, W.M. Bundy, and C. Harvey, eds., The Clay Minerals Society, Boulder, Colorado, 75–98.

Downs, R.T., Bartelmehs, K.L., Gibbs, G.V., and Boisen, M.B. (1993) Interactive software for calculating and displaying X-ray or neutron powder diffractometer patterns of crystalline materials. *American Mineralogist,* **78,** 1104–1107.

Doyle, L.J., Carder, K.L., and Steward, R.G. (1983) The hydraulic equivalence of mica. *Journal of Sedimentary Petrology,* **53,** 643–648.

Dydak, S.M. (1991) The hydraulic sorting of light and heavy minerals, heavy-mineral concentrations, and grain size. M.S. thesis, College of William and Mary, Williamsburg, Virginia. 90 pp.

Hathaway, J.C. (1956) Procedure for clay mineral analysis used in the sedimentary petrology laboratory of the U.S. Geological Survey. *Minerals Bulletin,* **3,** 8–13.

Hurst, V.J. (1997) Origins of the kaolins and associated bauxites. In *11th International Clay Conference Guidebook for the Field Trip to the Macon Area, Georgia,* S.M. Pickering Jr., V.J. Hurst, and J.M. Elzea, eds., Association Internationale pour l'Etude des Argiles, Ottawa, Canada, 32–46.

Hurst, V.J. and Pickering, S.M. (1997) Origin and classification of coastal-plain kaolins, southeastern USA, and the role of groundwater and microbial action. *Clays and Clay Minerals,* **45,** 274–285.

Hurst, V.J., Schroeder, P.A., and Styron, R.W. (1997) Accurate quantification of quartz and other phases by powder X-ray diffractometry. *Analytica Chimica Acta,* **337,** 233–252.

Kampf, N. and Schwertmann, U. (1982) Quantitative determination of goethite and hematite in kaolinitic soils by X-ray diffraction. *Clay Minerals,* **17,** 359–363.

Krumm, S. (1998) WinFit! v11.2. Computer Program for fitting peaks. Institut für Geologie Schlossgarten 5, Erlangen, Germany, 91054.

Melear, N.D. (1998) Crystal properties of goethite and hematite from three weathering profiles of the Georgia Piedmont. Ph.D. thesis, Department of Geology, University of Georgia, Athens, Georgia. 115 pp.

Pavich, M.J. (1989) Regolith residence time and the concept of surface age of the Piedmont ''peneplain''. *Geomorphology,* **2,** 181–196.

Raiswell, R. and Canfield, D.E. (1996) Rates of reaction between silicate iron and dissolved sulfide in Peru margin sediments. *Geochimica et Cosmochimica Acta,* **60,** 2777–2787.

Schwertmann, U., Friedl, J., Pfab, G., and Gehring, A.U. (1995) Iron substitution in soil and synthetic anatase. *Clays and Clay Minerals,* **43,** 599–606.

Shaw, W.H.R. (1960) Studies in biogeochemistry—I: A biogeochemical periodic table: The data. *Geochimica et Cosmochimica Acta,* **19,** 196–207.

Shiflet, J.E. (1999) Ti-bearing phases in an east-Georgia kaolin deposit. M.S. thesis, University of Georgia, Department of Geology, Athens, Georgia. 78 pp.

Singh, B. and Gilkes, R.J. (1991) Concentration of iron oxides from soil clays by 5 M NaOH treatment: The complete removal of sodalite and kaolin. *Clay Minerals,* **26,** 463–472.

Walker, R.G. (1992) Facies, facies models and modern stratigraphic concept: Facies models response to sea level change. In *Facies Models,* R.G. Walker and N.P. James, eds., Geological Association of Canada, St. Johns, New Foundland, Canada, 1–14.

Weaver, C.E. (1976) The nature of TiO_2 in kaolinite. *Clays and Clay Minerals,* **24,** 215–218.

E-mail of corresponding author: schroe@gly.uga.edu

(*Received 12 April 1999; accepted 17 September 1999; Ms. 333; A.E. Richard L. Hay*)